Angle-Resolved Spectroscopy of Positronium Emission from a Cu(110) Surface

A. C. L. Jones,[*] H. J. Rutbeck-Goldman, T. H. Hisakado, A. M. Piñeiro, H. W. K. Tom, and A. P. Mills, Jr.
Department of Physics and Astronomy, University of California Riverside, Riverside, California 92521, USA

B. Barbiellini
Department of Physics, Northeastern University, Boston, Massachusetts 02115, USA

J. Kuriplach
*Department of Low Temperature Physics, Faculty of Mathematics and Physics, Charles University,
V Holešovičkách 2, CZ-180 00 Prague, Czech Republic*

The affinity A_{Ps} of positronium (Ps) atoms for a metal is the negative of the maximum kinetic energy with which Ps is emitted into vacuum when thermalized positrons in a metal encounter the surface. When this quantity is measured by ground state Ps time of flight (TOF), the precision is severely limited by the short triplet state lifetime of 142 ns. By quickly converting the emitted Ps atoms into long-lived Rydberg states, we are able to dramatically increase the TOF to allow precision measurements of A_{Ps}. From our measurements made on a Cu(110) sample at $T = 128$ K, we find $A_{Ps}(128 \text{ K}) = (-2.476 \pm 0.010_{stat} \pm 0.013_{syst})$ eV, compared with the result $A_{Ps}(128 \text{ K}) = (-2.545 \pm 0.010_{num} \pm 0.010_{syst})$ eV found using highly accurate generalized gradient approximations for both electrons and positrons within density functional theory. Such precision opens up opportunities in the quest for an improved density functional.

Depending on the magnitudes of the electron and positron work functions [1], it may be energetically allowed for a thermal energy positron inside a metal to capture an electron and escape from the surface as a positronium (Ps) atom [2,3] while conserving total energy and the component of momentum parallel to the surface. At zero temperature the maximum Ps kinetic energy is the negative of the Ps affinity for the solid, which is the Ps ground state binding energy ($\frac{1}{2}R_\infty = 6.8028\ldots$ eV) less the sum of the electron and positron chemical potentials [4], $-A_{Ps} = \frac{1}{2}R_\infty - \mu_+ - \mu_-$. A_{Ps} is therefore a bulk property of a crystal and is amenable to density functional theory (DFT) calculations and experiments without complications from having to account for either intrinsic or extrinsic surface properties.

The model for Ps emission suggested by Platzman [5] posits that this process should occur predominantly leaving a single hole behind in the solid [see Fig. 1(a)] as is the case for ordinary electron photoemission illustrated in Fig. 1(b). In photoemission, there are substantial contributions to the observed line shape due to both discrete [6] and continuum [7] energy loss processes. We note that it is likely that analogous processes will occur in Ps emission [8], though perhaps with lower amplitudes due to the neutrality of the emitted atom. The Ps emission process is the exact analogue of the formation of a Cooper pair in Andreev reflection [9–11] [see Fig. 1(c)] and similar to the formation of an exciton by electrons and holes incident upon a

semiconductor *p-n* junction [Fig. 1(d)]. It is thus possible that angle-resolved Ps emission spectroscopy could provide a faithful map of the electronic density of states in a metal near the Fermi energy. With sufficient precision and the use of spin-polarized positrons [12–14], Ps emission spectroscopy could prove to be a valuable complement to ARPES, the vastly successful spin- and angle-resolved photoemission spectroscopy technique [15].

The first angle-resolved Ps emission experiments [16] using the 2D-ACAR [17–20] technique showed that the Ps emission spectra from clean Al surfaces map the electronic density of states near the sample surface, with the Fermi energy corresponding to Ps emitted with 2.5 eV of kinetic energy. However, the 13° full width at half maximum (FWHM) angular resolution and the 1 eV FWHM energy resolution for the Fermi energy Ps were not sufficient to justify further measurements [21]. In this Letter we describe our first experiments with an improved spectrometer having an angular resolution (3° FWHM) and time of flight (TOF) [22] energy resolution (~20 meV FWHM) comparable to what is achieved in ARPES. Aside from being a different way to gather information about the spin-dependent electronic structure of solids, the new experiments described here can provide precision measurements of A_{Ps} for comparisons with DFT [23–28]. In light of the facts that (1) the positron correlation energy contribution beyond the local density approximation is small and (2) there is no surface dipole contribution to the affinity of a neutral particle [29,30], such precision comparisons
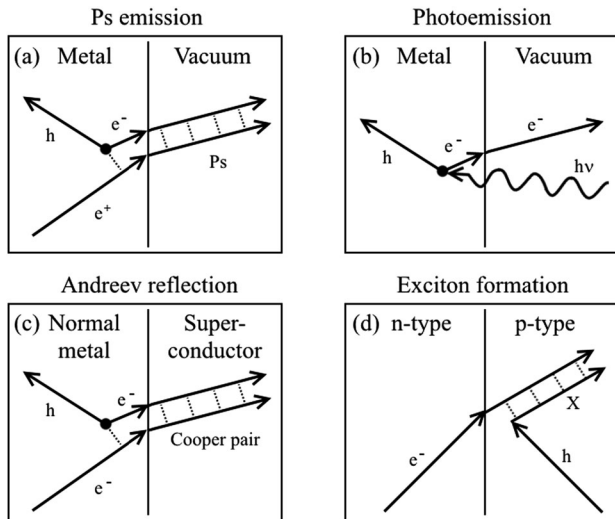
FIG. 1.   Conceptual drawings of the trajectories of various particles involved in positronium (Ps) emission analogs. The vertical lines in the centers represent the interface between a metal and the vacuum and between two different materials. (a) Ps emission and (b) photoelectron emission from a metal surface; (c) Andreev reflection process which creates a Cooper pair at the interface between a normal metal and a superconducter; (d) exciton (X) formation by electron and hole recombination at a p-n junction in a semiconductor.

could be valuable in the search for the most effective density functional in the quest to improve material property calculations over a wide range of fields [30–34].

In our experiment we produce Ps by implanting positrons with kinetic energies between 3–5.2 keV into a Cu(110) target. Beta decay in a ^{22}Na source ($\sim$10 mCi) in conjunction with a solid Ne moderator [35], produces a beam of $\sim 1 \times 10^6$ slow (few eV) positrons per second. A buffer gas trap [36] is used to collect and dump positrons at a rate of $\sim$0.2 Hz in pulses of 10^5 particles lasting $\sim$5 ns FWHM. A pulsed high voltage accelerator is used to provide the positrons with up to 5 keV of additional kinetic energy. As shown in Fig. 2, the positrons impinge on a Cu(110) target that is tilted such that Ps atoms emitted perpendicular to the surface can be detected at a distance L by a pair of ionizing grids and a microchannel plate (MCP) detector. To allow the use of a long L required for accurately measuring the emitted Ps energy distribution, we use lasers to excite the Ps into long-lived Rydberg states [37–39]. The state preparation is a two-step process, starting with excitation of the $1^3S - 2^3P$ transition followed by excitation to a Stark-split state of principal quantum number $n \sim 30$.

The two lasers used in this work are Nd:YAG pumped dye systems, very similar to those described in Ref. [40]. These provide up to $\sim$1 mJ/pulse of ultraviolet (UV) and $\sim$3 mJ/pulse of infrared (IR) light. Both lasers are tunable, but for the present experiments the UV laser was fixed at the Ps Lyman alpha wavelength (243.02 nm), while the IR
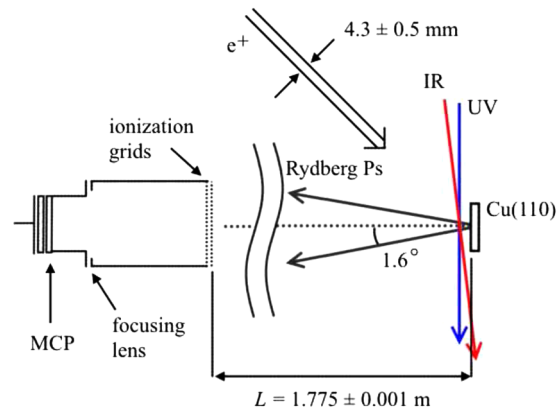

FIG. 2.   Experimental schematic detailing the geometry of the positron implantation, laser excitation, and Ps detection. The positron beam had a nearly rectangular distribution of $\sim$4.3 mm width. Two pulsed lasers fired in near coincidence with the positron implantation excite emitted Ps atoms to high Rydberg states. Rydberg Ps atoms emitted almost uniformly in a conical section of 1.6° half-angle normal to the target surface may reach the outermost grid of the detector after a flight path of $L = 1.775$ m.

wavelength was fixed at $\sim$732 nm, in a region of level spacings narrower than the laser bandwidth. The temporal width of both laser pulses was $\sim$5 ns. The two lasers were fired after the positron pulse with the timing adjusted across a range of $\sim$10 ns in order to cover the entire spectrum of Ps emission velocities.

The Cu(110) sample was prepared by etching in a solution of HNO_3, H_2PO_4, and glacial acetic acid, in a ratio of $1.5:1:1$. The sample was then mounted on a variable temperature cryostat, installed in a UHV chamber ($P < 10^{-9}$ torr), and heated to 900 K for 10 h to remove most of the surface contaminants. Note that small amounts of surface contaminants do not affect the Ps affinity since a change in the surface dipole potential changes the electron and positron work functions by equal and opposite amounts [4,29]. The IR and UV beams were directed nearly parallel to the sample surface to greatly reduce the first-order Doppler shifts for the Ps atoms emitted in the direction of the detector, as shown in Fig. 2.

Rydberg Ps atoms are detected at the end of a flight path $L = 1.775 \pm 0.001$ m, the termination of which is defined by the outermost grid of the detector, as shown in Fig. 2. The zero of time is determined from the prompt γ-ray signal produced at the surface of the MCP, measured with the lasers off over a period of $\sim$2 days. The 0.056% uncertainty in the flight path leads to a $\pm$0.11% systematic uncertainty in the energies, about $\pm$3 meV at 2.5 eV. The detector ionizes Rydberg atoms in a region of large electric field created between two 90% transmitting, 90 line per inch, Ni grids separated by 3.175 mm. Freed positrons are subsequently accelerated and focused onto the 42 mm diameter active face of a Hammamatsu 1217-21S MCP detector. The output of the detector anode is recorded on an oscilloscope

(Lecroy HDO4054) and saved with a time resolution of 2 ns on a computer. Analysis performed off-line after the experiment determined the flight times as the time elapsed from the prompt γ-ray signal from the arrival of positrons at the target to the time when the detector signal rises above a threshold that is selected to optimize the signal to noise ratio. The times of flight are corrected for the calculated delay (11.5 ± 0.5 ns) between ionization of Rydberg Ps at the grids and the arrival of the freed positron at the input face of the MCP, and for the γ-ray delay in traveling from the target to the MCP (~ 5.92 ns).

In Figs. 3(a)–3(d) we present measurements of the energy spectra of spontaneous Ps emission from Cu in the direction perpendicular to the surface $\pm 1.6°$. The data plotted have been collected with the target held at average temperatures of 120, 128, 298, and 532 K. In each data set the count rate initially rises gradually with increasing Ps energy, reaching a plateau followed by a sharp decline in signal in the vicinity of 2.5 eV. The observed spectra are consistent with the spontaneous formation of Ps as
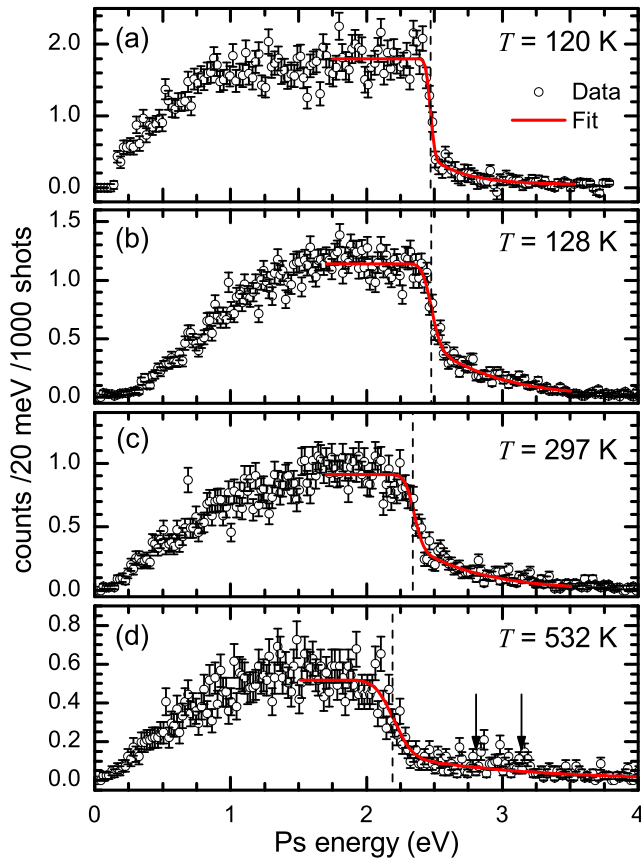

FIG. 3. Spontaneous Ps emission energy spectra for an implantation energy of 5 keV at target temperature (a) 120 K and 3 keV at target temperatures of (b) 128 K, (c) 297 K, and (d) 532 K. Solid lines illustrate fits of Eq. (2) to the data. Dashed vertical lines indicate the 50% cutoff point of the edge as determined from the fits. Arrows in plot (d) indicate a region of data excluded from the fit due to background signal.

thermalized positrons reach the Cu surface and pick up electrons from the Fermi sea. Under the assumption of a constant matrix element for this process, the emission rates are proportional to the product of the electron density of states and the emitted Ps density of states, $N(E_{Ps}) \propto \sqrt{E_{Ps}} \times \theta(E_S - E_{Ps})$ [5]. The data are in qualitative agreement with this simple model. Steps observed in the spectra are thus images of the Fermi surface in the direction perpendicular to the Cu(110) sample. The Ps energy E_S at the midpoint of the step is the negative of the Ps affinity,

$$E_S = \frac{1}{2}R_\infty - \mu_+ - \mu_- = -A_{Ps}. \qquad (1)$$

The tail following the step corresponding to the Fermi energy observed in each data set is attributed to incomplete thermalization of positrons. Increasing the positron implantation energy from 3 keV in Fig. 3(b) to 5 keV in Fig. 3(a) increases the implantation depth of the positrons and diminishes the relative proportion of counts occurring in the tail [41].

Because of the large velocity spread of the emitted Ps atoms (0–7×10^5 m/s), coupled with the short duration of the excitation laser pulses (~ 5 ns FWHM) it is not possible to accurately measure the positronium TOF distribution with a single delay interval between the positron implantation and laser firing times. The laser beams were aligned nearly parallel to the face of the target. A knife edge was placed in the UV laser path to cut off the light 1–2 mm in front of the target to minimize the background due to ions generated at the detector by scattered light. The combination of positioning the lasers a small distance in front of the target and the short duration of the pulses meant that it was not possible to excite emitted Ps evenly across the entire range of energies with a single time delay between the positron implantation and firing of the laser. Prior to the collection of the energy distribution data, the laser delay was scanned over a broad range of times to determine the range of time delays required to fairly sample the Ps energy distributions. The data sets presented in Fig. 3 each represent a sum over sets of scans taken as the delay is varied at 2 ns intervals between the onset of counts up to the delay resulting in the peak total signal. Although it is likely that this procedure will result in some distortion in the measured spectra, as the Fermi energy step is a relatively sharp feature, the observed positions of the steps should remain unaffected by the distortion. A background signal may result from the production of ions due to scattered UV radiation creating photoelectrons inside the detector assembly, which are then accelerated to 1–2 keV before colliding with the grid or walls of the detector, where they may ionize adsorbed gases from the surface, releasing heavy, positively charged ion species. The background, obtained from scans where the laser is fired just prior to the
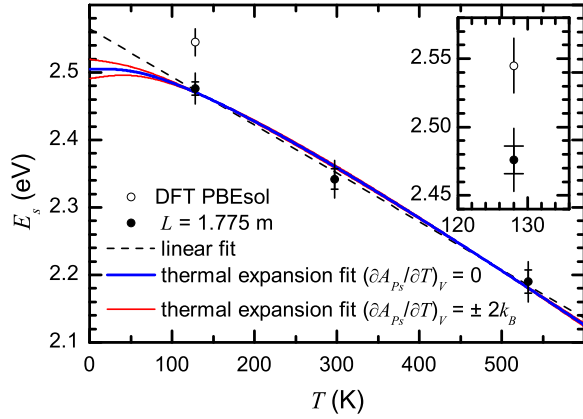
FIG. 4. DFT calculation at 128 K and measurements of the Ps Fermi energy cutoff, E_S for a Cu(110) surface as a function of temperature. From E_S we obtain the Ps affinity $A_{Ps} = -E_S$. Statistical errors are indicated by horizontal line segments, while the vertical error bars indicate the systematic error estimates.

Ps emission, is typically very small in the data of Fig. 3 except for panel (d), where a small background peak is possibly present between the arrows.

In Fig. 4 the cutoff energies E_S, indicating the Ps step energies, are plotted as a function of the target temperature. Note that the 5 keV datum [Fig. 3(a)] is not included in Fig. 4 because of a large uncertainty in L for that measurement. The cutoffs have been determined by fitting the region about the step in each of the spectra in Fig. 3 with a cutoff function (constructed from the complementary error function, erfc), plus a tail described by an exponential decay multiplied by an inverse cutoff function with the same center and width:

$$N(E) = A\left[\frac{1}{2}\mathrm{erfc}\left(\frac{E - E_S}{\sqrt{2}\sigma}\right)\right]$$
$$+ B\left[1 - \frac{1}{2}\mathrm{erfc}\left(\frac{E - E_S}{\sqrt{2}\sigma}\right)\right]\exp\left(\frac{-(E - E_S)}{\epsilon}\right).$$
$$(2)$$

Here the two components share a common step energy, E_S, leaving only the width σ, magnitudes A and B, and the characteristic decay energy ϵ of the epithermal tail as additional free variables. The widths of the steps $\Delta E_S = 2\sqrt{2\log 2}\sigma$ are found to be consistent with the free electron model values $\Delta E_S \approx 4k_B T$.

The measurement at 128 K is $E_s(128\ \mathrm{K}) = (2.476 \pm 0.010_{\mathrm{stat}} \pm 0.013_{\mathrm{syst}})$ eV, where the systematic error is given as the sum of the estimated error due to the TOF distance plus the error due to the time zero uncertainty. This experimental value can be compared directly with the result of our DFT calculations. Using the methodology described in Ref. [26] for a parameter-free model [27] for gradient-corrected electron-positron correlations, taking the

lattice constant known [42] for Cu at 128 K, and considering the so-called PBEsol [31] generalized gradient approximation (GGA) functional for electrons, we obtained for $-A_{Ps}$ a value of $(2.545 \pm 0.010_{\mathrm{num}})$ eV. The error of ± 0.010 eV is an estimated numerical uncertainty in our calculations [26]. This value must be corrected using the partial derivative of the affinity with respect to T at constant V,

$$-A_{Ps}(128\ \mathrm{K})$$
$$= 2.545\ \mathrm{eV} - \left(\frac{\partial A_{Ps}}{\partial T}\right)_V \times 128\ \mathrm{K}$$
$$= (2.545 \pm 0.010_{\mathrm{num}} \pm 0.010_{\mathrm{syst}})\ \mathrm{eV}, \quad (3)$$

where the partial derivative $(\partial A_{Ps}/\partial T)_V$ [43] is of the order of $\pm k_B$ and is treated as a systematic uncertainty added to the computational uncertainty. The final value of A_{Ps} compares well with its experimental counterpart. In fact, PBEsol gives more accurate equilibrium properties of densely packed solids compared to all other GGA schemes [31]. We note that the systematic uncertainty due to the poorly known $(\partial A_{Ps}/\partial T)_V$ will be reduced to a few meV by performing measurements over a range of low temperatures (e.g., $10 < T < 50$ K).

In order to benchmark other exchange-correlation schemes, we have examined the two most frequently used functionals, the GGA PBE functional [25] and the simple local density approximation (LDA) functional based on quantum Monte Carlo simulations for the homogeneous electron gas [44,45]. The calculated values of $-A_{Ps}$ at 128 K considering the temperature correction as above are $(2.762 \pm 0.010_{\mathrm{num}} \pm 0.010_{\mathrm{syst}})$ eV for the GGA PBE functional and $(2.196 \pm 0.010_{\mathrm{num}} \pm 0.010_{\mathrm{syst}})$ eV for the LDA functional. Therefore, the PBE functional overestimates $-A_{Ps}$, whereas the LDA functional considerably underestimates it. In the case of LDA calculations we employed an LDA electron-positron correlation functional by Drummond *et al.* [46] (on which the parameter-free gradient-corrected model [27] is built). Clearly PBEsol gives a better agreement with the experiment. The PBE overcorrections to LDA are in line with similar findings which have motivated the recent development of fully constrained meta-generalized-gradient approximations (meta-GGA) [28]. The positron part of calculations based on the parameter-free GGA model [27] seem to provide an accurate description at the GGA level. We conclude that further improvements can be expected when both the electrons and the positron are treated within strongly constrained meta-GGA schemes.

The average total derivative of A_{Ps} between 128 K and 532 K is found to be (0.72 ± 0.04) meV/K from the linear fit (dashed line in Fig. 4), in good agreement with the value 0.73 meV/K reported by Rosenberg *et al.* [47]. The three curves in Fig. 4 are fits to the three data points of the

volume expansion of Cu [48,49] with the partial derivative assumed to be 0 and $\pm 2k_B$.

We conclude that angle resolved Ps emission spectroscopy can provide a precise benchmark for DFT functionals and has the possibility of becoming a useful complement to angular resolved photoemission spectroscopy.

---

*adric.jones@ucr.edu

[1] P. J. Schultz and K. G. Lynn, Rev. Mod. Phys. **60**, 701 (1988).

[2] C. H. Hodges and M. J. Stott, Phys. Rev. B **7**, 73 (1973).

[3] K. F. Canter, A. P. Mills, Jr., and S. Berko, Phys. Rev. Lett. **33**, 7 (1974).

[4] D. W. Gidley and W. E. Frieze, Phys. Rev. Lett. **60**, 1193 (1988).

[5] A. P. Mills, Jr., L. Pfeiffer, and P. M. Platzman, Phys. Rev. Lett. **51**, 1085 (1983).

[6] N. V. Smith and W. E. Spicer, Phys. Rev. Lett. **23**, 769 (1969).

[7] P. H. Citrin, G. K. Wertheim, and Y. Baer, Phys. Rev. B **16**, 4256 (1977).

[8] A. P. Mills, Jr., E. D. Shaw, R. J. Chichester, and D. M. Zuckerman, Phys. Rev. B **40**, 8616 (1989).

[9] A. F. Andreev, Zh. Eksp. Teor. Fiz. **46**, 1823 (1964).

[10] A. F. Andreev, Sov. Phys. JETP **19**, 1228 (1964).

[11] P. A. M. Benistant, H. van Kempen, and P. Wyder, Phys. Rev. Lett. **51**, 817 (1983).

[12] S. Berko and J. Zuckerman, Phys. Rev. Lett. **13**, 339 (1964).

[13] D. W. Gidley, A. R. Köymen, and T. W. Capehart, Phys. Rev. Lett. **49**, 1779 (1982).

[14] D. B. Cassidy, V. E. Meligne, and A. P. Mills, Jr., Phys. Rev. Lett. **104**, 173401 (2010).

[15] J. H. Dil, J. Phys.: Condens. Matter **21**, 403001 (2009).

[16] D. M. Chen, S. Berko, K. F. Canter, K. G. Lynn, A. P. Mills, Jr., L. O. Roellig, P. Sferlazzo, M. Weinert, and R. N. West, Phys. Rev. Lett. **58**, 921 (1987).

[17] S. Berko and J. Mader, Appl. Phys. **5**, 287 (1975).

[18] S. Selvakumar, K. Sivaji, A. Arulchakkarvarthi, and S. Sankar, Phys. Chem. Chem. Phys. **16**, 15934 (2014).

[19] S. B. Dugdale, Low Temp. Phys. **40**, 328 (2014).

[20] H. Ceeh, J. A. Weber, P. Böni, M. Leitner, D. Benea, L. Chioncel, H. Ebert, J. Minár, D. Vollhardt, and C. Hugenschmidt, Sci. Rep. **6**, 20898 (2016).

[21] Note that even with the best angular resolution ever achieved, 0.1 mrad [P. Kubica and A. T. Stewart, Can. J. Phys. **61**, 971 (1983)], the energy resolution at the maximum Ps momentum (4 mrad) corresponds to 0.13 eV, about 10 times greater than the resolution achieved in the present results.

[22] A. C. L. Jones, H. J. Goldman, Q. Zhai, P. Feng, H. W. K. Tom, and A. P. Mills, Jr., Phys. Rev. Lett. **114**, 153201 (2015).

[23] P. Hohenberg and W. Kohn, Phys. Rev. **136**, B864 (1964).

[24] W. Kohn and L. J. Sham, Phys. Rev. **140**, A1133 (1965).

[25] J. P. Perdew, K. Burke, and M. Ernzerhof, Phys. Rev. Lett. **77**, 3865 (1996).

[26] J. Kuriplach and B. Barbiellini, Phys. Rev. B **89**, 155111 (2014).

[27] B. Barbiellini and J. Kuriplach, Phys. Rev. Lett. **114**, 147401 (2015).

[28] J. Sun, A. Ruzsinszky, and J. P. Perdew, Phys. Rev. Lett. **115**, 036402 (2015).

[29] N. D. Lang and W. Kohn, Phys. Rev. B **3**, 1215 (1971).

[30] J. P. Perdew and A. Ruzsinszky, Int. J. Quantum Chem. **110**, 2801 (2010).

[31] J. P. Perdew, A. Ruzsinszky, G. I. Csonka, O. A. Vydrov, G. E. Scuseria, L. A. Constantin, X. Zhou, and K. Burke, Phys. Rev. Lett. **100**, 136406 (2008).

[32] A. A. Hassanali, J. Cuny, V. Verdolino, and M. Parrinello, Phil. Trans. R. Soc. A **372**, 20120482 (2014).

[33] T. van Mourik, M. Bühl, and M.-P. Gaigeot, Phil. Trans. R. Soc. A **372**, 20120488 (2014).

[34] R. Peverati and D. G. Truhlar, Phil. Trans. R. Soc. A **372**, 20120476 (2014).

[35] A. P. Mills, Jr. and E. M. Gullikson, Appl. Phys. Lett. **49**, 1121 (1986).

[36] R. G. Greaves, M. D. Tinkle, and C. M. Surko, Phys. Plasmas **1**, 1439 (1994).

[37] K. P. Ziock, R. H. Howell, F. Magnotta, R. A. Failor, and K. M. Jones, Phys. Rev. Lett. **64**, 2366 (1990).

[38] D. B. Cassidy, T. H. Hisakado, H. W. K. Tom, and A. P. Mills, Jr., Phys. Rev. Lett. **108**, 043401 (2012).

[39] A. Deller, A. M. Alonso, B. S. Cooper, S. D. Hogan, and D. B. Cassidy, Phys. Rev. A **93**, 062513 (2016).

[40] D. B. Cassidy, T. H. Hisakado, V. E. Meligne, H. W. K. Tom, and A. P. Mills, Jr., Phys. Rev. A **82**, 052511 (2010).

[41] A. P. Mills, Jr., P. M. Platzman, and B. L. Brown, Phys. Rev. Lett. **41**, 1076 (1978).

[42] K. Wang and R. R. Reeber, High Temp. Mater. Sci. **35**, 181 (1996).

[43] B. K. Panda, C. D. Beling, and S. Fung, Phys. Rev. B **50**, 5695 (1994).

[44] D. M. Ceperley and B. J. Alder, Phys. Rev. Lett. **45**, 566 (1980).

[45] J. P. Perdew and Y. Wang, Phys. Rev. B **45**, 13244 (1992).

[46] N. D. Drummond, P. López Ríos, R. J. Needs, and C. J. Pickard, Phys. Rev. Lett. **107**, 207402 (2011).

[47] I. J. Rosenberg, R. H. Howell, and M. J. Fluss, Phys. Rev. B **35**, 2083 (1987).

[48] F. C. Nix and D. MacNair, Phys. Rev. **60**, 597 (1941).

[49] D. B. Fraser and A. C. Hollis Hallett, Can. J. Phys. **43**, 193 (1965).